

Supplementary Material:

“Three-in-one” Nano hybrids as Synergistic Nanoquenchers to Enhance No-Wash Fluorescence Biosensors for Ratiometric Detection of Cancer Biomarkers

Xiaolin Huang^{1,2#}, Zhimei He^{3,2#}, Dan Guo³, Yijing Liu², Jibin Song², Bryant C. Yung², Lisen Lin², Guocan Yu², Jun-Jie Zhu^{3*}, Yonghua Xiong^{1*}, and Xiaoyuan Chen^{2*}

¹State Key Laboratory of Food Science and Technology, Nanchang University, Nanchang 330047, P. R. China;

²Laboratory of Molecular Imaging and Nanomedicine (LOMIN), National Institute of Biomedical Imaging and Bioengineering (NIBIB), National Institutes of Health (NIH), Bethesda, Maryland 20892, United States

³State Key Laboratory of Analytical Chemistry for Life Science, School of Chemistry and Chemical Engineering, Nanjing University, Nanjing 210023, P. R. China

[#]These authors contributed equally to this work.

*Correspondence to:

Dr. Jun-Jie Zhu

State Key Laboratory of Analytical Chemistry for Life Sciences, School of Chemistry and Chemical Engineering, Nanjing University, Nanjing, P.R. China

E-mail: jjzhu@nju.edu.cn

Dr. Yonghua Xiong

State Key Laboratory of Food Science and Technology, and Jiangxi-OAI Joint Research Institute, Nanchang University

Address: 235 Nanjing East Road, Nanchang 330047, P.R. China

Phone: +0086-791-8833-4578. Fax: +0086-791-8833-3708

E-mail: yhxiongchen@163.com

Dr. Xiaoyuan Chen

Laboratory of Molecular Imaging and Nanomedicine (LOMIN), National Institute of Biomedical Imaging and Bioengineering (NIBIB), National Institutes of Health (NIH)

Address: Bethesda, Maryland 20892, United States

Phone: 301-451-4246

E-mail: shawn.chen@nih.gov

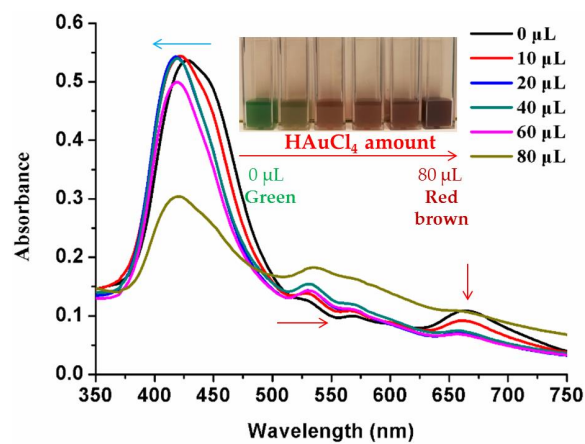


Figure S1 UV-visible absorption spectrum analysis for optimization of HAuCl₄ amounts in the preparation of MOF@AuNP.

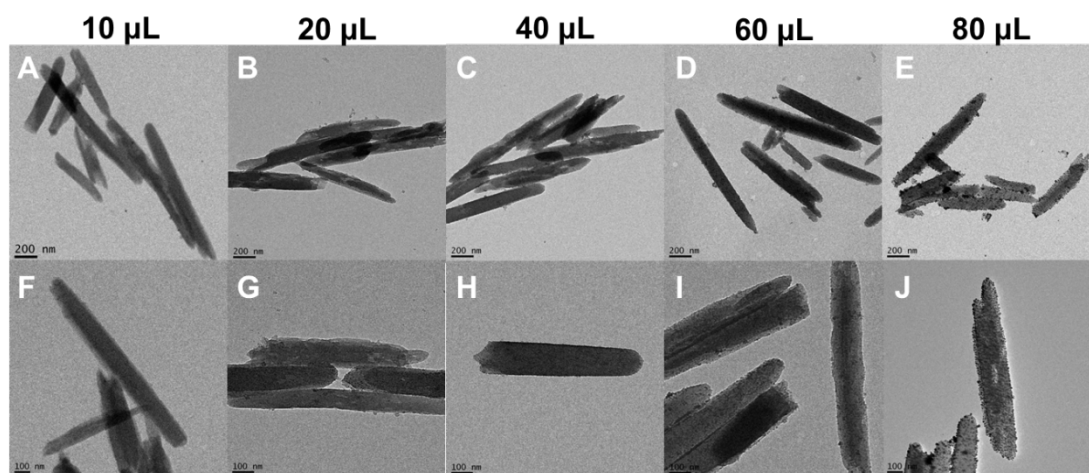


Figure S2 TEM imaging analysis for optimization of HAuCl_4 amounts in the preparation of MOF@AuNP at a concentration of 10 mg/mL with different volumes, including 10 μL (A and F), 20 μL (B and G), 40 μL (C and H), 60 μL (D and I), and 80 μL (E and J).

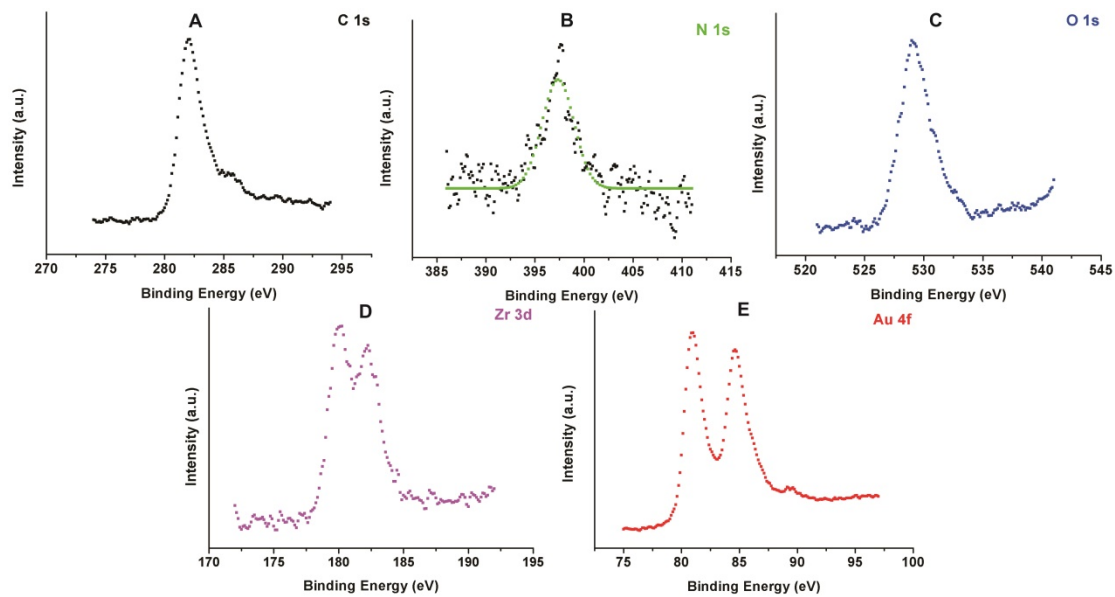


Figure S3 XPS spectrum analysis of MOF@AuNP. High-resolution XPS spectra of C 1s (A), N 1s (B), O 1s (C) Zr 3d (D) and Au 4f (E).

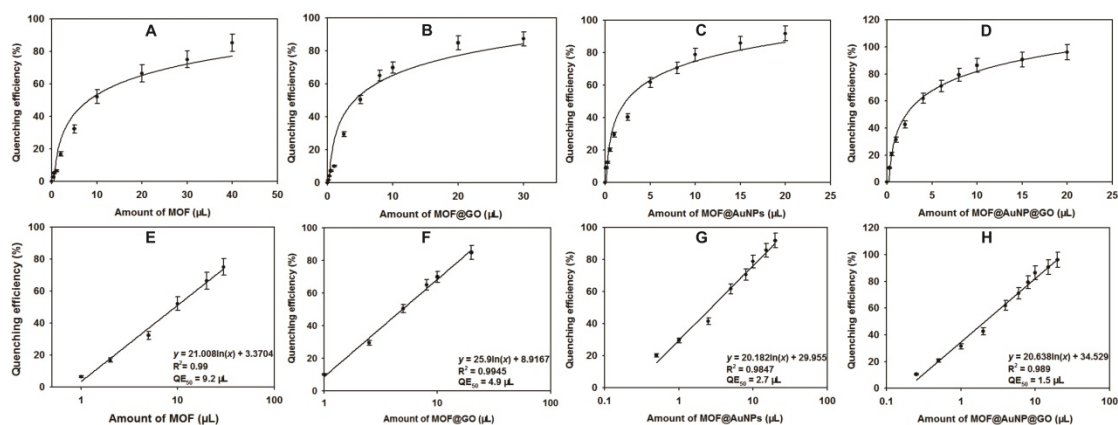


Figure S4 Comparison of fluorescence quenching efficiency of FAM-labeled ssDNA (1 nM) by using four MOF-based nanoquenchers, including MOF (A and E), MOF@GO (B and F), MOF@AuNP (C and G), and MOF@AuNP@GO (D and H) at the same MOF concentration of $25 \mu\text{g mL}^{-1}$, respectively. Fluorescence quenching efficiency (QE) was calculated using the following equation: $\text{QE (\%)} = (F_0 - F)/F_0 \times 100\%$, where F_0 and F are the fluorescence intensity of FAM-labeled ssDNA in the absence and presence of nanoquenchers, respectively. The value of QE_{50} was used to compare the fluorescence quenching ability of these four MOF-based nanostructures, where QE_{50} is the required nanoquencher amount with the fluorescence quenching efficiency at 50%. Amongst these four nanoquenchers, MOF@AuNP@GO showed the lowest required amount, with a QE_{50} of $1.5 \mu\text{L}$ compared with the other three nanomaterials, which indicated that the MOF@AuNP@GO exhibited the strongest fluorescence quenching ability. Moreover, the maximum fluorescence quenching efficiencies for MOF, MOF@GO, MOF@AuNP, and MOF@AuNP@GO were $81.08 \pm 3.07\%$, $89.29 \pm 1.86\%$, $92.87 \pm 2.51\%$, and $98.84 \pm 2.81\%$ at the nanoquencher amounts of 40, 30, 20, and 20 μL , respectively.

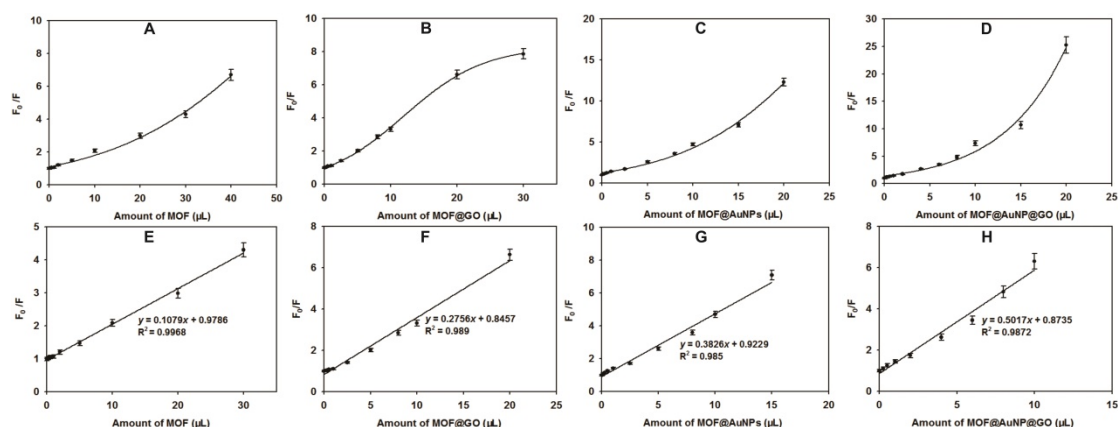


Figure S5 Stern-Volmer plots of FAM-labeled ssDNA (1 nM) quenching by varying amounts of MOF-based nanoquenchers including MOF alone (A and E), MOF@GO (B and F), MOF@AuNP (C and G), and MOF@AuNP@GO (D and H) at the same MOF concentration of $25 \mu\text{g mL}^{-1}$, respectively. Stern-Volmer equation: $F_0/F = 1 + K_{SV}[Q]$, where F_0 and F are the fluorescence intensity of FAM-labeled ssDNA in the absence and presence of nanoquenchers, respectively; K_{SV} is the Stern-Volmer quenching constant; and $[Q]$ is the concentration of the nanoquenchers. Here, the concentrations of four MOF-based nanoquenchers are the same at $25 \mu\text{g mL}^{-1}$, and the curve slopes represent the K_{SV} values. According to this picture, we can find among these four nanoquenchers, MOF@AuNP@GO possesses the largest curve slope of 0.5, indicating that MOF@AuNP@GO exhibits the strongest fluorescence quenching ability relative to the other three nanomaterials.

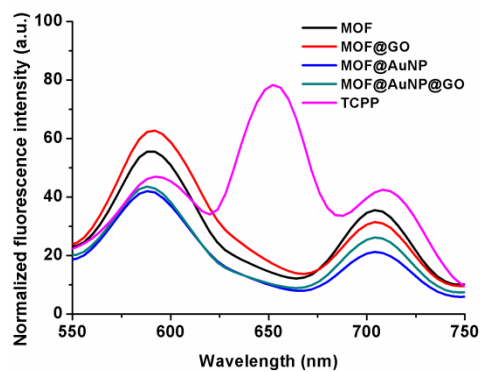


Figure S6 Fluorescence spectra of MOF, MOF@GO, MOF@AuNP, MOF@AuNP@GO, and TCPP in aqueous solution, with an excitation of 485 nm. Compared with the free TCPP, all four MOF-based nanostructures exhibited two blue-shifted fluorescence emissions at 594 nm and 704 nm, respectively. Additionally, the typical fluorescence emission at 650 nm from TCPP disappeared with the Zr-MOF synthesis. These results indicated the presence of TCPP in the developed Zr-MOF nanostructures.

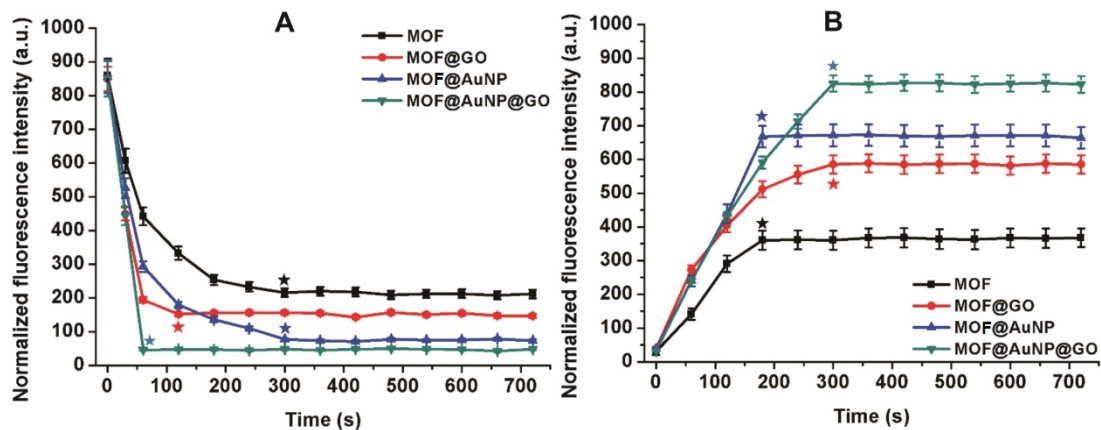


Figure S7 Kinetic study for time-dependent fluorescence changes of FAM-labeled ssDNA under the presence of different nanoquenchers. (A) Fluorescence quenching analysis of FAM-labeled ssDNA by these four MOF-based nanoquenchers, and (B) Fluorescence recovery analysis of the prepared FAM-labeled ssDNA/nanoquencher complex by target DNA (p53 gene) at the concentrations of 0.8, 8, 8, and 8 nM, respectively.

Detection of BRCA1 gene by using our proposed fluorescence biosensor based on MOF@AuNP@GO

Toward this end, the complementary Cy5-labeled ssDNA was designed as a fluorescence probe of BRCA1 gene, and the developed MOF@AuNP@GO with the highest quenching efficiency was selected as the fluorescence nanoquencher. The fluorescence spectra of Cy5-labeled ssDNA probe under different experimental conditions were recorded with an excitation at 633 nm, and results were shown in Figure S8. As illustrated, the Cy5-labeled ssDNA probe exhibits a strong fluorescence emission at 662 nm. However, the significant fluorescence quenching with the QE of $95.5 \pm 1.53\%$ was observed in the presence of MOF@AuNP@GO. Subsequently, with the addition of target BRCA1 gene, an obvious fluorescence recovery was obtained due to the formation of dsDNA that can detach from nanoquencher surface. These results indicate our developed nanosensor can also determine the presence of target BRCA1 gene. Figure S9A indicates fluorescence spectra of Cy5-labeled ssDNA probe at different concentrations of target, where the fluorescence emission intensity at 662 nm gradually increased with the increase of target BRCA1 gene concentrations, and an unchanged fluorescence emission at 840 nm was observed and used as a reference fluorescence signal for ratiometric measurement. By using the ratio of $I_{662\text{nm}}/I_{840\text{nm}}$ as a signal readout, the corresponding variations of ratiometric fluorescence signal against target concentrations were presented in Figure S9B, and an excellent linear relationship between the ratio of $I_{662\text{nm}}/I_{840\text{nm}}$ and target concentrations was obtained ranging from 0.001 to 5 nM with a LOD of 0.001 nM

(S/N = 3) (Figure S9C). This LOD was close to that obtained for p53 gene detection.

These above findings demonstrated the feasibility of our proposed fluorescence biosensor for detecting other cancer-related gene biomarkers.

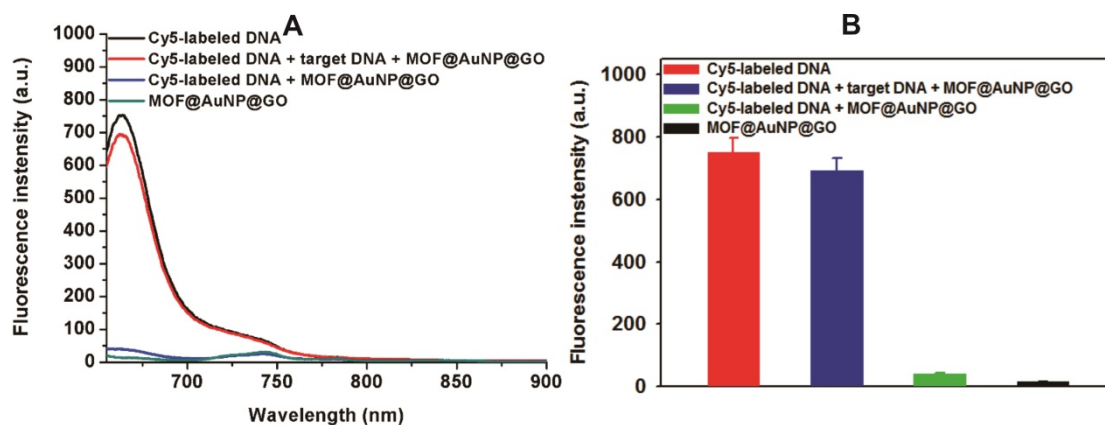


Figure S8 Fluorescence spectrum assay under different experimental conditions, including Cy5-labeled DNA probe, Cy5-labeled DNA probe + MOF@AuNP@GO, Cy5-labeled DNA probe + target BRCA1 gene + MOF@AuNP@GO, and MOF@AuNP@GO (A), and the corresponding fluorescence intensities (B). The concentrations of FAM-labeled DNA probe, target BRCA1 gene, and MOF@AuNP@GO in the final solution are 1 nM, 2 nM, and 2.5 $\mu\text{g mL}^{-1}$, respectively. Fluorescence spectra were collected with an excitation of 633 nm and an emission of 662 nm.

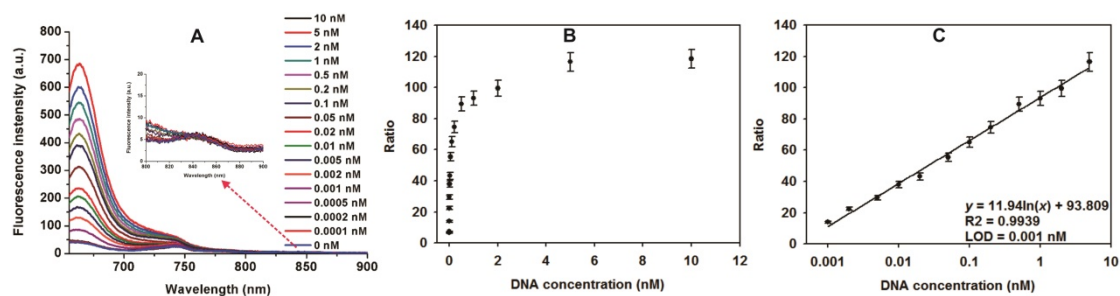


Figure S9 Fluorescence spectra of MOF@AuNP@GO in the presence of different concentrations of target BRCA1 gene (A), the corresponding relationships between the ratio of $I_{662\text{nm}}/I_{840\text{nm}}$ and target concentrations (B), and the corresponding calibration curves at low target concentrations (C). All experiments were carried out at 37 °C in 10 mM Tris-HCl buffer (pH 7.4, containing 100 mM NaCl, 5 mM KCl and 5 mM MgCl_2) with the concentration of MOF@AuNP@GO at $2.5 \mu\text{g mL}^{-1}$. Fluorescence spectra were collected with an excitation of 633 nm. Error bars were obtained from three repeated experiments.

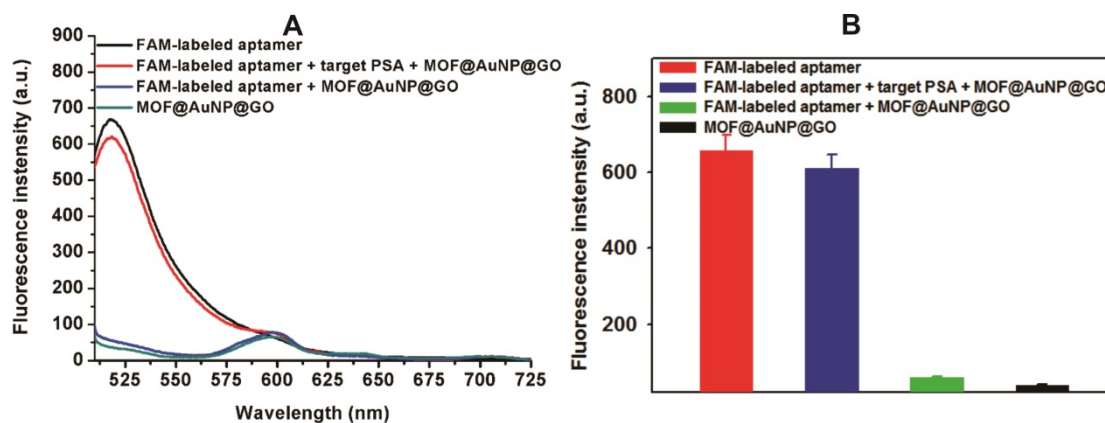


Figure S10 Fluorescence spectrum assay under different experimental conditions, including FAM-labeled aptamer probe, FAM-labeled aptamer probe + MOF@AuNP@GO, FAM-labeled aptamer probe + target PSA protein + MOF@AuNP@GO, and MOF@AuNP@GO (A), and the corresponding fluorescence intensities (B). The concentrations of FAM-labeled aptamer probe, target PSA protein, and MOF@AuNP@GO in the final solution are 1 nM, 20 ng mL⁻¹, and 2.5 μg mL⁻¹, respectively. Fluorescence spectra were collected with an excitation of 485 nm and an emission of 516 nm, respectively.

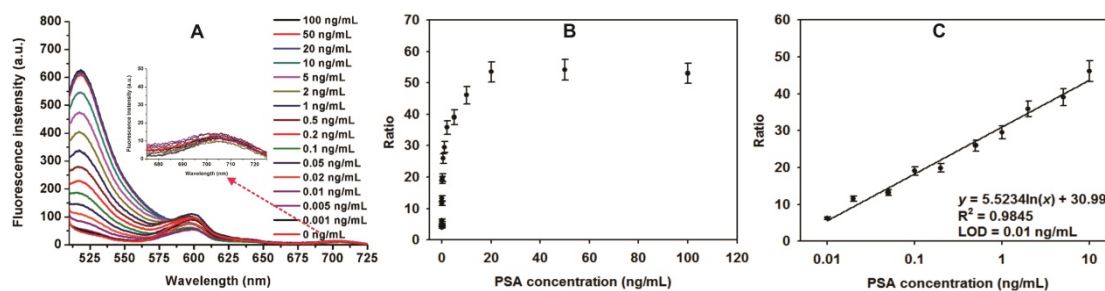


Figure S11 Fluorescence spectra of MOF@AuNP@GO in the presence of different concentrations of target PSA protein (A), the corresponding relationships between the ratio of $I_{516\text{nm}}/I_{704\text{nm}}$ and target concentrations (B), and the corresponding calibration curves at low target concentrations (C). All experiments were carried out at 37 °C, 20 mM, pH 7.4 Tris-HCl buffer solution with the concentration of MOF@AuNP@GO at $2.5 \mu\text{g mL}^{-1}$. Fluorescence spectra were collected with an excitation of 485 nm. Error bars were obtained from three repeated experiments.

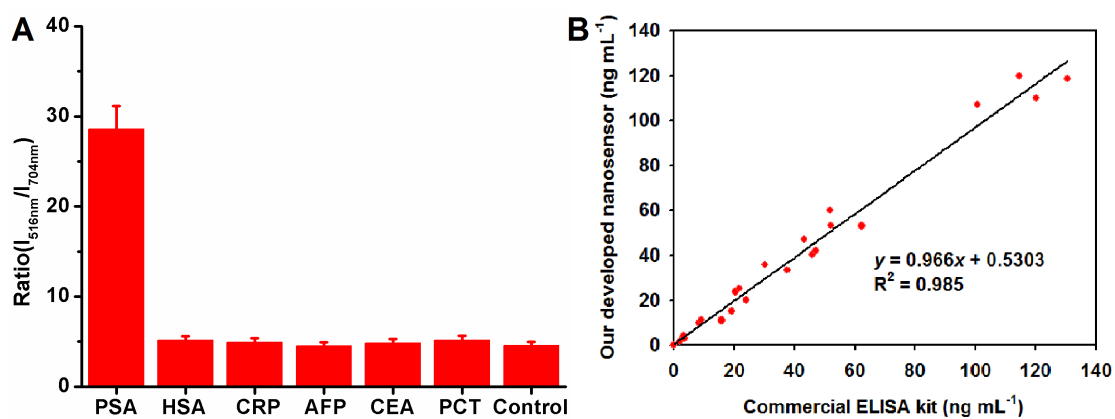


Figure S12 Specificity assay of our designed fluorescence biosensor using PSA (1 ng/mL), and other common protein biomarkers at 10 ng/mL including HSA, CRP, AFP, CEA and PCT, respectively. In addition, a negative sample was used as control only using FAM-labeled aptamer probe and MOF@AuNP@GO (A), and a correlation analysis of our proposed fluorescence nanosensor with a commercial ELISA kit method for PSA quantitative detection in thirty independent human serum samples with the PSA concentrations ranging from 0 to 120 ng mL⁻¹, respectively (B).

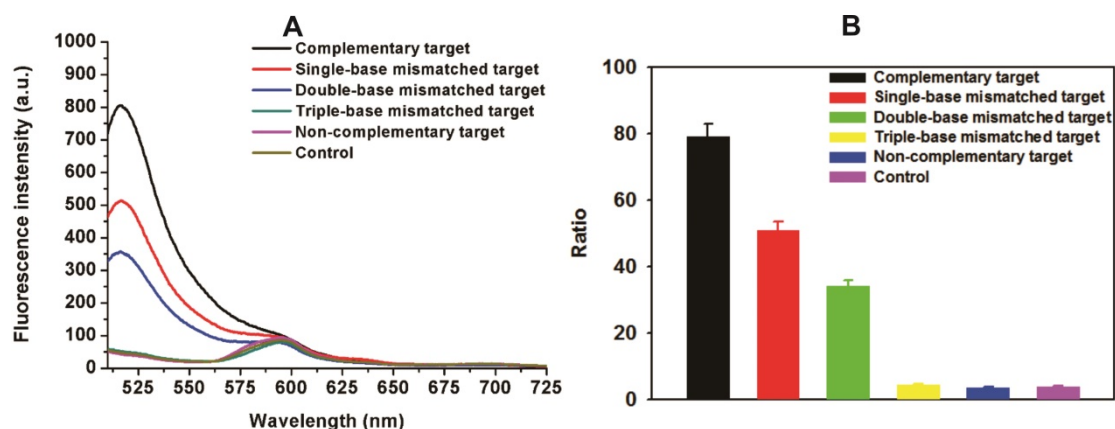


Figure S13 Fluorescence emission spectra of FAM-labeled DNA probe (P) under different conditions: (1) FAM-labeled p53 gene probe + MOF@AuNP@GO + complementary target p53 gene (T); (2) FAM-labeled p53 gene probe + MOF@AuNP@GO + single-base mismatched target p53 gene (T1); (3) FAM-labeled p53 gene probe + MOF@AuNP@GO + double-base mismatched target p53 gene (T2); (4) FAM-labeled p53 gene probe + MOF@AuNP@GO + triple-base mismatched target p53 gene (T3); (5) FAM-labeled p53 gene probe + MOF@AuNP@GO + non-complementary target (T4); and (6) Control (FAM-labeled p53 gene probe + MOF@AuNP@GO). The concentrations of T, T1, T2, T3, and T4 are 10 nM. The concentrations of FAM-labeled p53 gene probe and MOF@AuNP@GO are 1 nM and 2.5 $\mu\text{g mL}^{-1}$, respectively. (B) The corresponding histograms for the ratio of $I_{516\text{nm}}/I_{704\text{nm}}$ from (A). Fluorescence spectra were collected with an excitation of 485 nm and an emission of 516 nm, respectively.

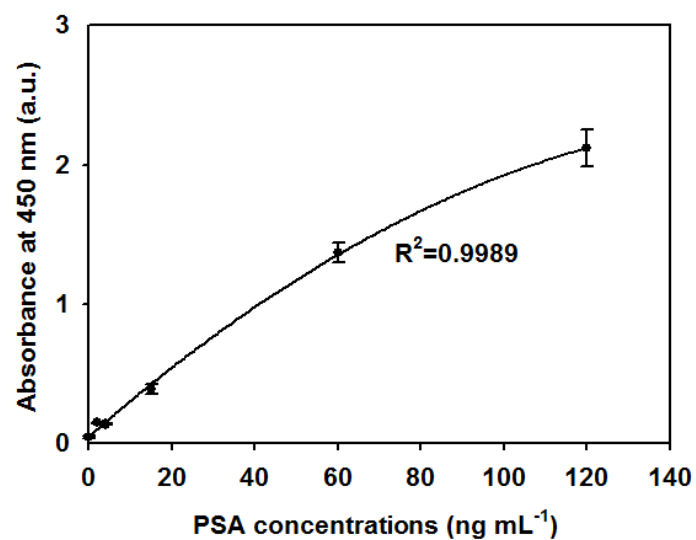


Figure S14. Standard curve of commercial ELISA kits for PSA detection at the concentrations ranging from 0 to 120 ng mL⁻¹. Error bars were obtained from three independent repeat experiments.

Table S1. DNA sequences employed in this study

Name	Sequence (5'-3')*
FAM-labeled P53 probe	CCTGGTGCCGTAGAT-FAM
Cy5-labeled BRCA1 probe	Cy5-GATTTTCTTCCTTTTGTTTC
FAM-labeled PSA aptamer probe	FAM-ATTAAAGCTCGCCATCAAATAGC TGC
Target p53 gene	ATCTACGGCACCAGG
Target BRCA1 gene	GAACAAAAGGAAGAAAATC
Single-base mismatch p53 gene (T1)	ATCTACGG <u>G</u> ACCAGG
Double-base mismatch p53 gene (T2)	ATCTA <u>G</u> GG <u>G</u> ACCAGG
Triple-base mismatch p53 gene (T3)	ATCTA <u>G</u> GG <u>G</u> A <u>C</u> GAGG
Non-complementary p53 gene (T4)	GCAGAGCTAGTTACA

*The mutated bases are in underlined and bolded text.

Table S2. Fluorescence intensity of Figure 3E in the main body of manuscript

No*	Nanoquencher type			
	MOF	MOF@GO	MOF@AuNP	MOF@AuNP@GO
1	829.1 ± 24.6	860.1 ± 25.8	890.2 ± 26.7	895.2 ± 21.3
2	764.5 ± 15.3	826.2 ± 16.5	847.8 ± 16.9	852.9 ± 17.0
3	237.5 ± 11.9	123.5 ± 6.2	57.6 ± 2.9	40.24 ± 2.0
4	61.6 ± 3.9	39.6 ± 2.0	43.9 ± 2.2	35.6 ± 1.8

*1, FAM-labeled DNA probe; 2, FAM-labeled DNA probe + target DNA + Nanoquenchers; 3, FAM-labeled DNA probe + Nanoquenchers; 4, Nanoquenchers.

Table S3. Comparison of existing nanoquencher-based no-wash fluorescent biosensors for target DNA detection

Nanoquencher type	Target	Sensitivity (nM)	Detection range (nM)	Detection time (min)	Multiplexed detection	Ref
ZIF-8 NP	HIV DNA	Not reported	2.5 to 1000	20	Not reported	[1]
Cu(H ₂ dtoa)	HIV DNA	3	10 to 100	240	Not reported	[2]
MIL-101	HIV-1 DNA	0.073	0.1 to 14	40	Not reported	[3]
Cu-MOF	HIV-1 DNA	0.073	0 to 50	30	Not reported	[4]
Zn-MOF	HIV-1 DNA	0.01	1 to 80	80	Not reported	[5]
MIL-88B nanorods	HIV DNA	0.01	0 to 5	4	Not reported	[6]
Cd(L)(HDMA) ₂ (DMF)(H ₂ O) ₃	DNA	0.05	0 to 125	Not reported	Not reported	[7]
2D Zn-TCPP nanosheets	H1N1, H5N1 DNA	0.02	0 to 5	5	Yes	[8]
TaS ₂ nanosheets	H1N1, H5N1 DNA	0.05	0 to 5	5	Yes	[9]
MoS ₂ nanosheets	DNA	0.05	0 to 50	Minutes	Not reported	[10]
Graphene oxide	DNA	0.1	0 to 25	1	Yes	[11]
Graphene oxide	DNA	0.00025	0 to 10	10	Not reported	[12]
g-C ₃ N ₄ nanosheets	DNA	0.081	0.2 to 30	30	Not reported	[13]
Graphdiyne nanosheets	H1N1, H5N1, M13 DNA	0.025	0 to 5	Instant	Yes	[14]
2D COF nanosheets	DNA	0.02	0 to 1	240	Not reported	[15]
Graphene oxide and AuNPs	HIV-1 DNA	0.000015	0.00005 to 1	5	Not reported	[16]
MoS ₂ nanosheets	p53	0.5	0 to 15	5	Not reported	[17]
Zr-MOF	p53	0.2	0.4 to 20	10	Yes	This work
Zr-MOF@GO	p53	0.08	0.1 to 20			
Zr-MOF@AuNP	p53	0.02	0.02 to 10			
Zr-MOF@AuNP@GO	p53	0.005	0.01 to 10			

Table S4. Recovery of p53 gene in human serum (n = 3)

Spiked p53 concentrations (nM)	Detected (nM)	Recovery (%)	Relative standard deviation (RSD, %)
0	—	—	—
0.1	0.092 ± 0.01	92	10.8
1	0.97 ± 0.09	97	9.28
5	5.17 ± 0.41	103.4	7.93
10	9.52 ± 0.69	95.2	7.25

Table S5. Comparison of our developed nanosensors with existing nanoquencher-based no-wash fluorescent biosensors and the widely-used commercial ELISA kits for PSA detection

Methods	Target	Sensitivity (ng mL ⁻¹)	Detection range (ng mL ⁻¹)	Detection time (min)	Ref
Existing nanoquencher-based no-wash fluorescent biosensors					
MoO ₃ nanosheets	PSA	0.4	0 to 4	40	[18]
MoS ₂ nanosheetS	PSA	0.2	0 to 60	40	[19]
Graphene oxide	PSA	0.05*10 ⁻⁶	(0.1 to 3) *10 ⁻⁶	120	[20]
Commercial ELISA kits					
Abnova Corporation.	PSA	Not reported	0 to 120	140	KA0208
Arigo biolaboratories Corp.	PSA	0.2	1.56 to 25	85	ARG80649
Elabscience Biotechnology Inc.	PSA	0.19	0.31~20	270	E-EL-H0091
Crystal Chem Inc.	PSA	0.1	0.5 to 100	Not reported	80976
Enzo Life Sciences, Inc.	PSA	0.024	0.12 to 28	150	ENZ-KIT146-0001
MyBioSource, Inc.	PSA	0.01	Not reported	75	MBS723076
Thermo Fisher Scientific Inc.	PSA	0.008	0.008 to 20	300	EHK3T
Abcam plc.	PSA	< 0.008	0.01 to 25	90	ab113327
Zr-MOF@AuNP@GO	PSA	0.01	0.05 to 10	35	This work

References:

1. Liu S, Wang L, Tian J, et al. Application of zeolitic imidazolate framework-8 nanoparticles for the fluorescence-enhanced detection of nucleic acids. *ChemPhysChem*. 2012; 77: 23-6.
2. Zhu X, Zheng H, Wei X, et al. Metal-organic framework (MOF): A novel sensing platform for biomolecules. *Chem Commun*. 2013; 49: 1276-8.
3. Fang JM, Leng F, Zhao XJ, et al. Metal-organic framework MIL-101 as a low background signal platform for label-free DNA detection. *Analyst*. 2014; 139: 801-6.
4. Yang S-P, Chen S-R, Liu S-W, et al. Platforms formed from a three-dimensional Cu-based zwitterionic metal-organic framework and probe ss-DNA: Selective fluorescent biosensors for human immunodeficiency virus 1 ds-DNA and sudan virus rna sequences. *Anal Chem*. 2015; 87: 12206-14.
5. Zhao H-Q, Qiu G-H, Liang Z, et al. A zinc (II)-based two-dimensional MOF for sensitive and selective sensing of HIV-1 ds-DNA sequences. *Anal Chim Acta*. 2016; 922: 55-63.
6. Tian J, Liu Q, Shi J, et al. Rapid, sensitive, and selective fluorescent DNA detection using iron-based metal-organic framework nanorods: Synergies of the metal center and organic linker. *Biosens Bioelectron*. 2015; 71: 1-6.
7. Wang G-Y, Song C, Kong D-M, et al. Two luminescent metal-organic frameworks for the sensing of nitroaromatic explosives and DNA strands. *J Mater Chem A*. 2014; 2: 2213-20.
8. Zhao M, Wang Y, Ma Q, et al. Ultrathin 2D metal-organic framework nanosheets. *Adv Mater*. 2015; 27: 7372-8.
9. Zhang Y, Zheng B, Zhu C, et al. Single-layer transition metal dichalcogenide nanosheet-based nanosensors for rapid, sensitive, and multiplexed detection of DNA. *Adv Mater*. 2015; 27: 935-9.
10. Huang Y, Shi Y, Yang HY, et al. A novel single-layered MoS₂ nanosheet based microfluidic biosensor for ultrasensitive detection of DNA. *Nanoscale*. 2015; 7: 2245-9.
11. He S, Song B, Li D, et al. A graphene nanoprobe for rapid, sensitive, and multicolor fluorescent DNA analysis. *Adv Funct Mater*. 2010; 20: 453-9.
12. Li J, Huang Y, Wang D, et al. A power-free microfluidic chip for SNP genotyping using graphene oxide and a DNA intercalating dye. *Chem Commun*. 2013; 49: 3125-7.
13. Wang Q, Wang W, Lei J, et al. Fluorescence quenching of carbon nitride nanosheet through its interaction with DNA for versatile fluorescence sensing. *Anal Chem*. 2013; 85: 12182-8.
14. Parvin N, Jin Q, Wei Y, et al. Few-layer graphdiyne nanosheets applied for multiplexed real-time DNA detection. *Adv Mater*. 2017; 29: 1606755.
15. Peng Y, Huang Y, Zhu Y, et al. Ultrathin two-dimensional covalent organic framework nanosheets: Preparation and application in highly sensitive and selective DNA detection. *J Am Chem Soc*. 2017; 139: 8698-704.
16. Qaddare SH, Salimi A. Amplified fluorescent sensing of DNA using luminescent carbon dots and AuNPs/GO as a sensing platform: A novel coupling of fret and DNA

hybridization for homogeneous HIV-1 gene detection at femtomolar level. *Biosens Bioelectron.* 2017; 89: 773-80.

17. Zhu C, Zeng Z, Li H, et al. Single-layer MoS₂-based nanoprobe for homogeneous detection of biomolecules. *J Am Chem Soc.* 2013; 135: 5998-6001.

18. Dhenadhayalan N, Yadav K, Sriram MI, et al. Ultra-sensitive DNA sensing of a prostate-specific antigen based on 2D nanosheets in live cells. *Nanoscale.* 2017; 9: 12087-95.

19. Kong R-M, Ding L, Wang Z, et al. A novel aptamer-functionalized MoS₂ nanosheet fluorescent biosensor for sensitive detection of prostate specific antigen. *Anal Bioanal Chem.* 2015; 407: 369-77.

20. Fang B-Y, Wang C-Y, Li C, et al. Amplified using Dnase I and aptamer/graphene oxide for sensing prostate specific antigen in human serum. *Sens Actuators B.* 2017; 244: 928-33.